High-speed linear detection time domain optical coherence tomography with reflective grating-generated spatial reference delay

Yuuki Watanabe,* Fumitoshi Sajima, Toshiki Itagaki, Kei Watanabe, and Yuuki Shuto

Faculty of Engineering, Yamagata University, 4-3-16 Johnan, Yonezawa, Yamagata, 992-8510, Japan

*Corresponding author: ywata@yz.yamagata-u.ac.jp

Received 8 January 2009; revised 18 April 2009; accepted 24 May 2009;
posted 28 May 2009 (Doc. ID 106016); published 18 June 2009

We developed a high-speed linear detection time-domain optical coherence tomography (OCT) technique that detected a reflective grating-generated spatial optical delay in the reference arm using a line scan camera during probe-beam scanning. Using an InGaAs line scan camera (512 pixels) operating at 47,000 lines/s, the calculation of the absolute value of the difference between two sequential lines can be approximately displayed as cross-sectional images with 500 lateral pixels at 94 frames/s. After data acquisition, we performed postprocessing that involves a Hilbert transform to improve the image quality of an OCT image. Our OCT system was successfully used to image a human finger *in vivo* with 93 dB sensitivity.

OCIS codes: 100.2000, 110.4500.

1. Introduction

Optical coherence tomography (OCT) is a noninvasive, noncontact imaging modality used to obtain high-resolution cross-sectional images of tissue structures [1]. Broadly speaking, OCT can be grouped into two categories: time-domain (TD)-OCT and Fourier-domain (FD)-OCT [2–6]. Conventional TD-OCT detects the echo time delays of light by measuring the interference signal as a function of time during a depth scan (A-scan) in a reference arm at each position of a probe beam scanning laterally in the sample arm. In FD-OCT, the mechanical A-scan in TD-OCT is replaced either by a spectrograph or by a swept-source system. FD-OCT allows greater sensitivity and faster imaging speeds than TD-OCT [4]. More recently, ultrahigh-speed FD-OCT techniques have been demonstrated using a Fourier-domain mode-locked laser at sweep rates of 370 kHz [5] and a complementary metal oxide semiconductor (CMOS) scan camera at A-scan rates of 312.5 kHz [6]. OCT images require mapping and interpolation of the axial data from wavelength- to k-space and the subsequent application of a Fourier transform. The standard FD-OCT image contains DC and conjugate artifacts, and suffers from a strong signal-to-noise ratio (SNR) fall-off, which is proportional to the distance from zero delay, and a sinc function reduction of the depth-dependent sensitivity because of the limited detection linewidth.

In order to realize a faster TD technique, we applied a nonmechanical scanning grating-generated coherence microscopic technique [7] to image biological tissues *in vivo* [8–11]. This technique obtains a 2D interference image (axial–lateral coordinate) of a sample during a short exposure with a 2D camera using diffracted light as a reference beam to generate a continuous spatial optical delay and a linear probe beam that is focused by a cylindrical lens. Although other techniques have been demonstrated using grating-based correlation and a 2D camera [12–14], the grating-generated coherence microscopic technique has a simpler optical layout. Using an

0003-6935/09/183401-06$15.00/0

ultrahigh-speed CMOS camera at 3000 frames/s (fps), we obtained OCT images (512 × 512 pixels) with a 5.8 mm × 2.0 mm (lateral × axial) imaging range at 1500 fps by calculating two sequential images [9]. In the case of a relatively slow indium gallium arsenide (InGaAs) camera (320 × 256 pixels, 60 fps, 1 ms exposure time), the calculation of the OCT image requires the elimination of the DC image from the interference images and the application of a 1D Hilbert transform to obtain a complex analytic signal in the axial direction [11]. The DC image contains the intensity of noninterfered light and the electrical noise of the camera. The imaging speed was limited by the frame rate of the InGaAs camera, and the resultant duty ratio (exposure time/frame interval time) of this system was only 6%. The use of a long exposure time causes fringe washout due to sample motion, resulting in a decrease of the SNR. Furthermore, the principle drawback of this technique is due to the linear focused probe beam: the lateral resolution is limited as a consequence of coherent cross talk and aberrations in the singlet cylindrical lens.

To overcome these problems, we demonstrate here a linear detection TD-OCT system with a reflective grating-generated spatial reference optical delay using a high-speed InGaAs line scan camera operating at 47,000 lines/s during conventional probe-beam scanning. Koch *et al.* have demonstrated a similar linear TD-OCT system that uses a transmission grating to detect the zero order diffraction of the probe beam and the first-order diffraction of the reference beam [15]. An OCT image (2.0 mm× 0.94 mm; lateral × axial) of human skin was obtained with 80 dB sensitivity and an A-scan rate of 1.2 kHz. Although our approach is not fundamentally different, we can distinguish between the use of a transmission grating and a reflective one. Because the optical path difference is double in the reflection geometry, a depth range can be obtained that is twice as large as in the transmission geometry by using the same grating pitch and the same wavelength. Approximate cross-sectional images (500 lateral pixels) with an imaging size of 4.0 mm × 2.6 mm (lateral × axial) can be displayed in real time at 94 fps by calculating the absolute value of the difference between data for two sequential lines. Furthermore, we performed postprocessing of the data to improve the image quality. We subtracted the reference intensity distribution, averaged over data for 500 lines, from data for each line, used a high-pass filter to reduce the incoherent components of a sample beam, and then applied a Hilbert transform to obtain an analytic signal. This system has sufficient sensitivity (93 dB with 47 kHz A-scan rate) to image biological tissues *in vivo*.

2. Experimental Setup and Optical Coherence Tomography Image Calculation

Figure 1 shows a schematic of the experimental setup. The collimated light of a superluminescent diode

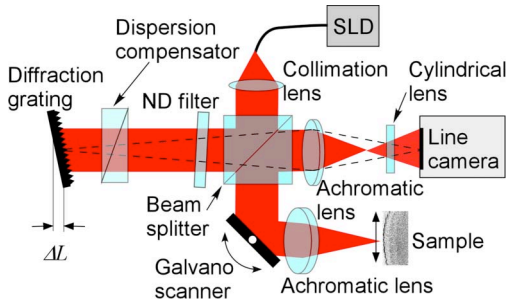

Fig. 1. (Color online) Schematic of linear detection time-domain optical coherence tomography. SLD, superluminescent diode; ND filter, neutral density filter; dashed line, imaging ray.

(Inphenix, SLD IPSDD1305; center wavelength $\lambda_0 = 1.33\,\mu$m, full width at half-maximum spectral width $\Delta\lambda = 57.6$ nm, coherence length $l_c = 27.1\,\mu$m) was split into the sample and reference arms by a nonpolarizing cube beam splitter. In the sample arm, the probe beam, which was focused on a sample by an achromatic lens ($f = 75$ mm), was scanned using a galvano scanner. A reflective diffraction grating was installed in the reference arm with the Littrow configuration. The Littrow angle θ is determined by

$$\theta = \sin^{-1}(n\lambda_0/2p), \tag{1}$$

where $p = 1/600$ mm is the spacing between the grooves and n is the diffraction order. We used first-order diffracted light, and the Littrow angle was $\theta = 23.5°$. The continuous spatial optical delay, ΔL, generated by the diffraction grating is given by

$$\Delta L = d\tan\theta, \tag{2}$$

where d is the beam diameter. The diffracted light from the grating was imaged on an InGaAs line scan camera (SUI Goodrich Corp., 512 pixels; 25 μm pixel, 14 bit resolution, 47,000 lines/s, exposure time 18.2 μs) by using an achromatic lens ($f = 150$ mm). The duty ratio (exposure time/line interval time) of this camera was 85.5%. The sample and reference beams were vertically focused on the line camera by a cylindrical lens. The camera output is described as

$$E = I_{\mathrm{ref}} + I_{\mathrm{sig}} + I_{\mathrm{inc}} + 2[I_{\mathrm{sig}}(x,z)I_{\mathrm{ref}} * |\gamma(z)|]^{1/2}\cos\phi(x,z), \tag{3}$$

where I_{ref}, I_{sig}, and I_{inc} are the intensities of the reference, sample, and incoherent light, respectively; $\gamma(z)$ is the amplitude of the modulation, which is determined by the coherence degree of the light source; ϕ is the phase difference between the sample and reference beams; and $*$ denotes the convolution operator.

With the TD techniques using a camera, an approximate cross section of a sample can be obtained by calculating the difference between the sequential camera outputs, as the intensity of the reference beam is a dominant factor in camera outputs for

imaging of biological samples [9]. In our system, the data for two sequential lines are axial data on different lateral positions, so the absolute value of the difference between two sequential lines contains the absolute value of the spatial gradient in the lateral direction. The result also includes the phase term and is therefore not a true OCT image. However, the absolute value of the spatial gradient appears similar to the OCT image because most biological samples have continuous structures in the lateral direction. Since the calculated result can be displayed in real-time, owing to the simplicity of the calculation, this method was used to find the imaging position of our samples.

We calculated more accurate OCT images using the following procedure. In order to extract only the interference component from the camera output, we subtracted the intensity distribution of the reference beam, which was estimated by averaging data from a sufficient number of lines in the lateral direction from the line data at each lateral position. A high-pass filter was then used to reduce the incoherent component of a sample beam, which is uniform in the axial direction. We obtained an analytic image, $f_A(x,z)$, from these data, $f(x,z)$, using a Hilbert transform. In the frequency domain, the analytic signal was derived from the input signal by suppressing its negative frequency components and multiplying the positive ones by two. This transforms a real-valued signal f into a complex-valued signal f_A. The real part of f_A is identical to the input signal, and the imaginary part is a $(-\pi/2)$-phase-shifted version (or the Hilbert transform f_H of f). Finally, the OCT image can be obtained as

$$S = f^2(x,z) + {f_H}^2(x,z) = 4[I_{\mathrm{sig}}(x,z) I_{\mathrm{ref}} * |\gamma(z)|]. \quad (4)$$

Although the 1D Hilbert transform can be performed in the axial or the lateral direction, we applied the Hilbert transform to the modulated signal in the lateral direction because fewer fringes occurred in the axial direction due to the diffractive grating. For imaging stationary samples without a lateral phase shift, we need the reference path modulation generated by moving the grating. To calculate OCT images, we performed the high-pass filtering in the axial direction and the Hilbert transform in the lateral direction simultaneously in the 2D frequency domain (shown in Fig. 2). If the number of pixels per coherence function is sufficient to resolve the axially modulated interference signal that is generated by the tilted reference wave, we can use the high-pass filter and the Hilbert transform in the axial direction simultaneously in the 1D frequency domain. Although the computation time can be improved by the use of 1D FFT instead of 2D FFT, the imaging depth is decreased by the limitation of the number of pixels in the line camera.

3. Results and Discussion

First, we estimated the sensitivity of the linear detection TD-OCT system. The SNR was measured experimentally by moving a plane mirror with a round-trip attenuation of 50 dB axially in 200 μm steps. To obtain the reference beam profile, we measured the modulated interference fringes (512×500 pixels) by oscillating the mirror using a piezoelectric transducer. Here we obtained the intensity distribution of the reference beam by averaging over data from 500 lines. The illumination power used was

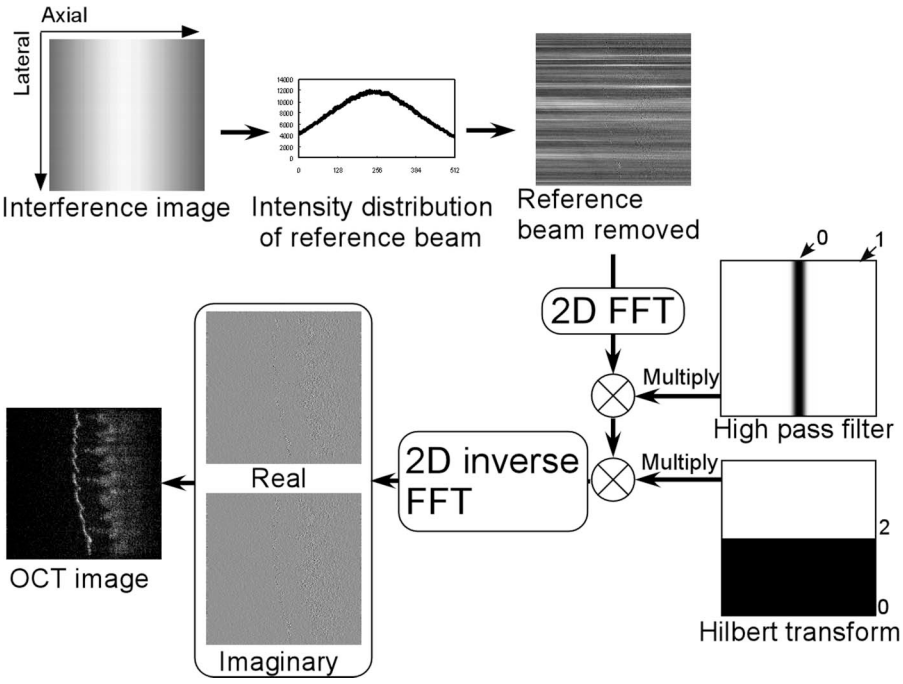

Fig. 2. Flow chart of the calculation of the OCT image using the Hilbert transform.

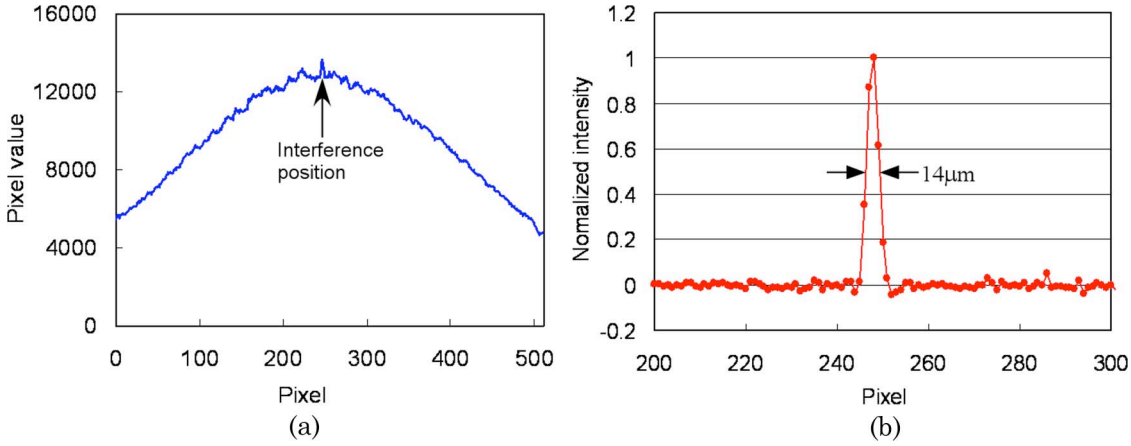

Fig. 3. (Color online) (a) Camera output, (b) demodulated axial profile.

about 3.0 mW on the sample arm. We used a neutral density filter to adjust the optical power of the reference beam until the pixel values were close to the saturation level of the camera. Figure 3 shows an example of the camera output and its demodulated profile. In Fig. 3(a), the intensity of the reference beam was a dominant factor in camera outputs because of the sample beam with 50 dB attenuation. This interference signal is similar to that of biological samples. The number of pixels per coherence function was approximately five. Figure 4 shows the axial profiles at different depths and the noise floor. The sensitivity was about 93 dB in the center region of the axial measurement range and decreased with distance from the center. This decrease was primarily due to the Gaussian beam profile. To obtain uniform sensitivity in the axial range, we require a top-hat beam profile. The axial resolution was about 14 μm in the center region of the axial range, which agreed with the theoretical value (13.6 μm), and fell to 17 μm away from the center. The axial resolution is not affected by the dispersion of the diffraction grating if the grating plane is optically conjugated with the plane of the camera. For this reason, the decrease in axial resolution was probably due to defocusing of the imaging lens.

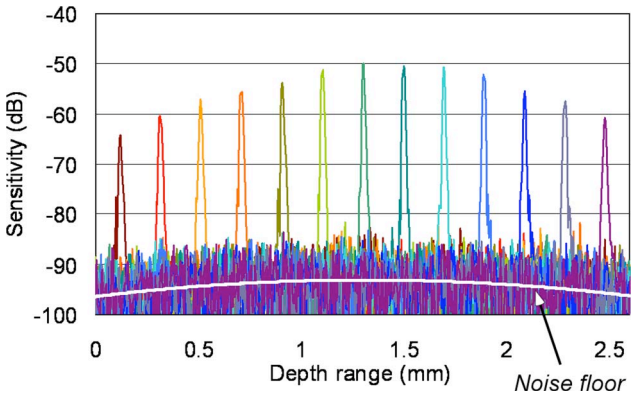

Fig. 4. (Color online) Sensitivities with an attenuation of –50 dB in the sample arm at different depths.

Next, we estimated the theoretical sensitivity of our system. In previous work [11], we introduced the minimum detectable reflectivity to estimate the theoretical sensitivity using the shot-noise-limited full field (FF) OCT system [16]. FF-OCT has the same illumination area at both the sample and the reference arm. In FF-OCT system, the minimum detectable reflectivity $R_{\mathrm{min-FF-OCT}}(\mathrm{SNR}=2)$ can be expressed as

$$R_{\mathrm{min-FF-OCT}} = \frac{(R_{\mathrm{ref}} + R_{\mathrm{inc}})^2}{R_{\mathrm{ref}}\xi_{\mathrm{max}}}, \tag{5}$$

where R_{ref} is the reflectivity of the reference mirror, R_{inc} is the proportion of incoherent light, and ξ_{max} is the maximum full-well capacity. Let the optical density at the sample be α times greater than at the reference. Because the objective lens focuses the probe beam in the linear detection TD-OCT system, the factor α influences the reflectivities on the sample arm only. Hence, the minimum detectable reflectivity $R_{\mathrm{min}-L-\mathrm{OCT}}$ can be expressed as

$$\alpha R_{\mathrm{min}-L-\mathrm{OCT}} = \frac{(R_{\mathrm{ref}} + \alpha R_{\mathrm{inc}})^2}{R_{\mathrm{ref}}\xi_{\mathrm{max}}}. \tag{6}$$

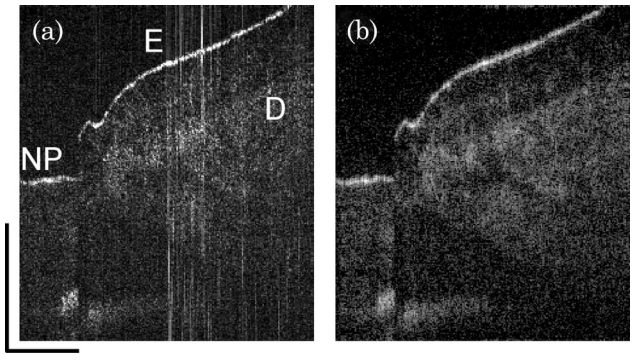

Fig. 5. *In vivo* OCT images of a human nail-fold region by (a) the absolute value in the difference between data for two sequential lines (Media 1), (b) demodulation with the Hilbert transform (Media 2). Imaging area, 4.0 mm × 2.6 mm(lateral × axial); NP, nail plate; E, epidermis; D, dermis; scale bar, 1 mm.

Our InGaAs line camera has a full-well capacity of $\xi_{\max} = 1.25 \times 10^6$ electrons. We measured the reference reflectivity to be $R_{\text{ref}} = 4.5\%$ when the reflectivity of a plane mirror was measured at 100%. The calculated beam width, w_0, at the waist was $w_0 = (4\lambda_0/\pi)(f/d) = 15.9\,\mu\text{m}$ for an incident beam diameter, d, of $d = 8.0\,\text{mm}$. Because both sample and reference beams were vertically focused on the line camera by a cylindrical lens, the intensity of the probe beam was $\alpha = d/w_0 \sim 5.1 \times 10^2$, which is greater than the intensity of the reference beam in the horizontal direction. The incoherent component of the signal light was negligible when a plane mirror was used as the sample. Therefore, the estimated theoretical sensitivity of our linear detection TD-OCT system is $10 \log(R_{\min\text{-}L\text{-}\text{OCT}}) \sim -101.5\,\text{dB}$. The experimental value was lower than the theoretical sensitivity, which may in part be attributed to losses in the sample arm optics.

Finally, we measured the OCT images of the nail-fold region of a human finger. The probe beam was scanned at 94 Hz using a saw tooth waveform with a duty cycle of 90%, which was modified to reduce mechanical vibrations. Figure 5(a) shows the calculated image, with an imaging range of a 4.0 mm × 2.6 mm (lateral × axial) using only the absolute values of the differences between data for sequential lines. Although we can see the internal structures at roughly 94 fps using the simple calculation, this image contains incoherent components in the sample beam in the axial direction and the phase term. Figure 5(b) shows the calculated OCT image with a logarithmic scale using the demodulation of the Hilbert transform. We can see an improvement in image quality; however, the axial profiles are blurred due to the filtering process. Using the high-frequency fringe of the interference signal generated by the tilted reference wave may improve the axial resolution.

The imaging speed of the linear detection TD-OCT system depends on the line scan camera and is the same as the SD-OCT system. However, the detection sensitivity is lower due to the nature of the TD technique. The computation time of the linear detection TD-OCT image (512 axial × 500 lateral pixels) with the demodulation of the Hilbert transform was similar to that of the standard SD-OCT image (512 axial × 500 lateral pixels), which contained a linear interpolation and 1D FFT (1024 points). In apractical SD-OCT system, the sample has to be carefully located below the zero-delay line to avoid overlapping between the real image and its conjugate mirror image. Because our OCT image is conjugate artifact free, we do not need be so careful with the sample location.

The OCT images with the demodulation of the Hilbert transform were not able to display in real time due to heavy calculations, which include 2D FFT and inverse FFT. More recently real-time holographic microscopy, which involves 2D FFT calculations, has been demonstrated using a graphic processing unit (GPU) with many stream processors [17]. In our next work, we are planning to accelerate the calculations of the OCT images by a GPU.

4. Conclusion

We have demonstrated a high-speed linear detection TD-OCT technique that detected a reflective grating-generated spatial optical delay in the reference arm using a line scan camera during probe-beam scanning. Using an InGaAs line scan camera (512 pixels) operating at 47 kHz, cross-sectional structures (500× 512 pixels) can be displayed at approximately 94 fps by calculating only the absolute value of the difference between two sequential line data. To improve image quality, we applied the Hilbert transform to obtain an OCT image from a 2D interference data. Our OCT system is a simple optical layout, artifact-free, high-speed (47 kHz A-scan), and sufficiently sensitive (93 dB) to image biological tissues *in vivo*.

This study was partially supported by a Grant-in-Aid for Scientific Research (20700375) from the Japan Society for the Promotion of Science (JSPS) and the Industrial Technology Research Grant Program in '05 from the New Energy and Industrial Technology Development Organization (NEDO) of Japan

References

1. D. Huang, E. A. Swanson, C. P. Lin, J. S. Schuman, W. G. Stinson, W. Chang, M. R. Hee, T. Flotte, K. Gregory, C. A. Puliafito, and J. G. Fujimoto, "Optical coherence tomography," Science **254**, 1178–1181 (1991).
2. A. F. Fercher, C. K. Hitzenberger, G. Kamp, and S. Y. El-Zaiat, "Measurement of intraocular distances by backscattering spectral interferometry," Opt. Commun. **117**, 43–48 (1995).
3. G. Häusler and M. W. Lindner, ""Coherence radar" and "spectral radar"–new tools for dermatological diagnosis," J. Biomed. Opt. **3**, 21–31 (1998).
4. R. Leitgeb, C. Hitzenberger, and A. Fercher, "Performance of fourier domain vs. time domain optical coherence tomography," Opt. Express **11**, 889–894 (2003).
5. R. Huber, D. C. Adler, and J. G. Fujimoto, "Buffered Fourier domain mode locking:unidirectional swept laser sources for optical coherence tomography imaging at 370,000 lines/s," Opt. Lett. **31**, 2975–2977 (2006).
6. B. Potsaid, I. Gorczynska, V. J. Srinivasan, Y. Chen, J. Jiang, A. Cable, and J. G. Fujimoto, "Ultrahigh speed spectral / Fourier domain OCT ophthalmic imaging at 70,000 to 312,500 axial scans per second," Opt. Express **16**, 15149–15169 (2008).
7. I. Zeylikovich, A. Gilerson, and R. R. Alfano, "Nonmechanical grating-generated scanning coherence microscopy," Opt. Lett. **23**, 1797–1799 (1998).
8. Y. Watanabe, K. Yamada, and M. Sato, "*In vivo* nonmechanical scanning grating-generated optical coherence tomography using an InGaAs digital camera," Opt. Commun. **261**, 376–380 (2006).
9. Y. Watanabe, K. Yamada, and M. Sato, "Three-dimensional imaging by ultrahigh-speed axial-lateral parallel time domain optical coherence tomography," Opt. Express **14**, 5201–5209 (2006).
10. Y. Watanabe, Y. Takasugi, K. Yamada, and M. Sato, "Axial-lateral parallel time domain OCT with optical zoom lens

and high order diffracted lights for variable imaging range," Opt. Express **15**, 5208–5217 (2007).
11. Y. Watanabe and M. Sato, "Quasi-single shot axial-lateral parallel time domain optical coherence tomography with Hilbert transformation," Opt. Express **16**, 524–534 (2008).
12. G. Brun, I. Verrier, A. Barthélémy, C. Froehly, and J. P. Goure, "Measurements of mode propagation time in multimode fibers using a real-time interferometric amplitude correlator," J. Opt. Commun. **13**, 134–139 (1992).
13. I. Zeylikovich and R. R. Alfano, "Ultrafast dark-field interferometric microscopic reflectometry," Opt. Lett. **21**, 1682–1684 (1996).
14. I. Verrier, G. Brun, and J. P. Goure, "SISAM interferometer for distance measurements," Appl. Opt. **36**, 6225–6230 (1997).
15. P. Koch, V. Hellemanns, and G. Hüttmann, "Linear optical coherence tomography system with extended measurement range," Opt. Lett. **31**, 2882–2884 (2006).
16. A. Dubois, L. Vabre, A. C. Boccara, and E. Beaurepaire, "High-resolution full-field optical coherence tomography with a Linnik microscope," Appl. Opt. **41**, 805–812 (2002).
17. T. Shimobaba, Y. Sato, J. Miura, M. Takenouchi, and T. Ito, "Real-time digital holographic microscopy using the graphic processing unit," Opt. Express **16**, 11776–11781 (2008).